


# A multi-functional genetic manipulation system and its use in high-level expression of a $\beta$ -mannanase mutant with high specific activity in *Pichia pastoris*

Zheming Liu, Linyuan Cao, Xiaodan Fu, Qingping Liang, Han Sun and Haijin Mou\*   
College of Food Science and Engineering, Ocean University of China, Qingdao, 266003, China.

## Summary

To further extend the practical application of a thermostable and acidic resistance  $\beta$ -mannanase (ManAK) in animal feed additives, an effective strategy that combined directed evolution and metabolic engineering was developed. Four positive mutants (P191M, P194E, S199G and S268Q) with enhanced specific activity (25.5%–60.9%) were obtained. The S199G mutant exhibited 56.7% enhancement of specific activity at 37°C and good thermostability, and this was selected for high-level expression in *P. pastoris* X33. A multi-functional and scarless genetic manipulation system was proposed and functionally verified (gene deletion, substitution/insertion and point mutation). This was then subjected to Rox1p (an oxygen related transcription regulator) deletion and *Vitreoscilla* haemoglobin (VHb) co-expression for high enzyme productivity in *P. pastoris* X33VIIManAK<sup>S199G</sup>. An excellent strain, named X33VIIManAK<sup>S199G</sup>  $\Delta$ rox1::VHb, was achieved by combining these two factors, and then the maximum enzymatic activity was further increased to 3753 U ml<sup>-1</sup>, which was nearly twice as much as the maximum production of ManAK in *P. pastoris*. This work provides a systematic and effective method to improve the enzymatic yield of  $\beta$ -mannanase, promotes the application of ManAK in feed additives, and also demonstrated that a scarless genetic manipulation tool is useful in *P. pastoris*.

## Introduction

In recent years,  $\beta$ -mannanases, one of the main hemicellulose enzymes, have attracted considerable attention

due to the increasing demand for sustainable and renewable bio-resources and their application within industrial areas (Yamabhai *et al.*, 2016).  $\beta$ -mannanases can be utilized for the preparation of manno-oligosaccharide (MOS) prebiotics by enzymatic hydrolysing plant cell walls (Srivastava and Kapoor, 2017; Srivastava *et al.*, 2017); eliminating anti-nutritional factors in corn soy-based feed (Dhawan and Kaur, 2007); and improving coffee extraction efficiency by decreasing viscosity (Sachslehner *et al.*, 2000). Additionally,  $\beta$ -mannanases are employed in the pulp and paper industry (Gübitz *et al.*, 1997), and for cleaning detergents and biofuels (Choi *et al.*, 2015).

$\beta$ -mannanase (EC 3.2.1.78), commonly known as an endo-acting enzyme, can randomly cleave (1→4)- $\beta$ -D-mannosidic bonds in the backbone of different mannans (Malgas *et al.*, 2015). According to the categories of the CAZY database ([www.cazy.org](http://www.cazy.org)),  $\beta$ -mannanases are divided into four glycoside hydrolase (GH) families, viz. 5, 26, 113 and 134. Most of the  $\beta$ -mannanases belong to the GH5 and GH26 families, and the remaining few are members of the GH113 and GH134 families. Some GH5 and GH113  $\beta$ -mannanases have transglycosylation activities, in which a carbohydrate hydroxyl acts as the acceptor to form MOS, or other mannosides, instead of water (Vocadlo and Davies, 2008).

ManAK is a thermophilic and acidophilic GH5 family  $\beta$ -mannanase from *Aspergillus Kawachii* IFO 4308. This enzyme has previously been demonstrated to display good potential for the preparation of MOS prebiotics from konjac gum, locust bean gum, and guar gum (Liu *et al.*, 2020). It is commonly recognized that thermostable and acidophilic enzymes are also desired in feed additives, since good thermal tolerance enables an enzyme to withstand the instantaneous high temperature required for the feed pelleting process. In addition, due to the acidic environment (pH 1.5–3.5) present within the digestive tract of monogastric animals, acidophilic enzymes that are able to retain high enzyme activities in an acidic pH range are welcomed (Zhang *et al.*, 2010). Therefore, we tried to further consider the potential utilization of ManAK in feed additives. Even though the maximum yield of ManAK that could be reached was 11,600 U ml<sup>-1</sup> under optimal conditions for enzymatic activity (75°C and pH 3.0) using high cell

Received 19 January, 2021; revised 23 March, 2021; accepted 29 March, 2021.

\*For correspondence. E-mail [mousun@ouc.edu.cn](mailto:mousun@ouc.edu.cn); Tel. +86-532 82032290; Fax +86 532 82032290.

*Microbial Biotechnology* (2021) 14(4), 1525–1538  
doi:10.1111/1751-7915.13812

© 2021 The Authors. *Microbial Biotechnology* published by John Wiley & Sons Ltd and Society for Applied Microbiology.

This is an open access article under the terms of the Creative Commons Attribution-NonCommercial-NoDerivs License, which permits use and distribution in any medium, provided the original work is properly cited, the use is non-commercial and no modifications or adaptations are made.

density fermentation (HCDF), the corresponding yield decreased to about 1900 U ml<sup>-1</sup> (37°C and pH 5.5) according to the Chinese Standards of  $\beta$ -mannanase for animal feed (GB/T36861–2018) (Liu *et al.*, 2020). This low yield would have a corresponding high production cost, and this hinders the practical utilization of ManAK in feed additives. In general, a high specific activity of enzyme and high protein productivity from the production strain are two key factors that determine the final enzymatic activity yield. Because higher specific activity of enzyme means more total enzymatic activity under the same protein yield, there is a continual need to improve the specific activity of ManAK.

Directed evolution methodology has proved to be a powerful method to redesign enzymes and enables researchers to engineer robust enzymes to meet the demands of industrial processes (Markel *et al.*, 2020). Furthermore, directed evolution has shown potential for unlocking novel enzymatic reactions, such as formation of C-Si and C-P bonds (Kan *et al.*, 2016, 2017). Unlike a rational design strategy, directed evolution methodology can uncover beneficial mutation sites that improve specific activity and that are far from the catalytic core of the enzyme (Zhang *et al.*, 2019). A computational-based rational design strategy normally predicts promising mutation candidates for specific activity changes, based upon enzyme-substrate docking results, and selects mutants from within the catalytic core (Cheng *et al.*, 2015; Tang *et al.*, 2018; Yin *et al.*, 2018). Thus, theoretically, a directed evolution methodology could give more diverse mutants that benefit enzymatic specific activity.

A high protein productivity of the production strain is the other key factor that determines the final enzymatic activity yield of industrial enzymes. There are a vast number of strategies for improving the protein productivity in *P. pastoris*, such as a multi-copy strategy (Teng *et al.*, 2015), optimizing promoters and integration events (Prielhofer *et al.*, 2013; Schwarzans *et al.*, 2016; Vogl *et al.*, 2018), facilitating protein folding and secretion (Li *et al.*, 2016), selecting proper host strains, HCDF, etc (Ahmad *et al.*, 2014). HCDF can increase the protein productivity in *P. pastoris* (Tolner *et al.*, 2006). During this process, oxygen demand is extremely high, and the oxygen supply critically influences the final protein yield (Wang *et al.*, 2012; Wu and Fu, 2012; Liu *et al.*, 2015; Zhao *et al.*, 2020). Co-expression of *Vitreoscilla* hemoglobin (VHb) seems to be a rational way to alleviate this problem. VHb was firstly discovered in the aerobic bacterium *Vitreoscilla* in the 1960s. A function study indicated that VHb tends to efficiently bind oxygen at low O<sub>2</sub> concentrations and deliver it to terminal respiratory oxidases, and this improves respiratory efficiency and ATP synthesis. High oxygen binding

and releasing ability makes it possible to alleviate the limitation of high oxygen demand during the HCDF process (Stark *et al.*, 2015). However, it is not necessarily correct that *P. pastoris* could yield higher level protein productivity under hypoxic conditions than under fully aerobic conditions. This has been confirmed by several recent studies and was partially ascribed to the transcriptional regulation by Rox1p. Under aerobic conditions, Rox1p can function as a heme-dependent transcription regulator that terminates the transcription of a series of hypoxia-induced genes. Further studies confirmed that knocking out of the Rox1p encoding gene (*rox1*) in yeast, could not only alter lipid classes that benefit protein secretion, but could also upregulate translation elongation factor ANB1 that accelerates protein synthesis in *P. pastoris* (Liu *et al.*, 2015; Martínez *et al.*, 2016).

Repeated genome editings, such as insertion, deletion, substitution, and point mutation of target genes, require powerful genetic manipulation tools. Resistant genes, which serve as conventional selectable markers for genetic manipulations, cannot provide multi-chromosomal loci editing, due to the unavailability of enough antibiotic-resistant marker genes (Dong and Zhang, 2014). Among four well-known markerless or scarless genetic editing systems, such as a site-specific-based recombination method, counter-selection system, phage recombinase-mediated ssDNA-directed system, and the CRISPR/Cas9 system, a counter-selectable system has been widely used for scarless genetic manipulation in *Bacillus* (Wu *et al.*, 2017). There are several advantages that might be responsible for this, such as completely scarless genetic manipulation (without leaving a specific redundant sequence), multi-functional (insertion, deletion, substitution, and point mutation), versatile and relative ease of manipulation (Lin *et al.*, 2013; Wu *et al.*, 2017). Considering classical genetic manipulation by homologous recombination using selection markers are most applied, it is necessary to develop similar scarless genetic manipulation system specifically for *P. pastoris* (Fischer and Glieder, 2019).

This study undertook a systemic strategy to develop cost-effective industrial enzymes, in terms of enhanced specific activity through directed evolution, and construction of a high protein productivity strain via genetic manipulation of *P. pastoris*. Specifically, at the first stage, the specific activity (at 37°C) of ManAK was enhanced by directed evolution to comply with the application requirement in animals. At the second stage, the best mutant was subjected to high level expression in *P. pastoris* using a multi-copy strategy, and optimizing oxygen-related metabolism regulation, via a versatile auxotrophic-antibiotic counter-selectable cassette (AACC) genetic manipulation system.

## Result and discussion

### Screening high specific activity mutants produced by directed evolution

For the purpose of enhancing the specific activity of ManAK at 37°C, an error-prone PCR-based directed evolution methodology was undertaken to construct a mutation library in *P. pastoris*. As described in Fig. 1, the mutation library was first constructed in *E. coli* DH5 $\alpha$ , in order to gain a collection of recombinant plasmids that were used for the sequential transformation and selection of positive mutants in *P. pastoris*. Approximately 10 000 clones were picked up and inoculated into 48-well deep plates for the first round of screening, during which the mutants showing > 20% higher enzymatic activity than the control group (~ 200 clones) were selected for the second round of screening. The second round of screening was also performed in 48-well deep plates to further confirm the

results from the first round of screening. From this, 120 clones were left for the third round of screening in 100-ml shake flasks, and 42 transformants showing enhanced enzymatic activity were used for preparation and purification of enzymes. Because these mutants were fusion proteins with 6xHis tags at the C-terminal end, the target protein was easily purified by the Ni-affinity chromatography method. Finally, four positive mutants (P191 M, P194E, S199G and S268Q) with enhanced specific activity were selected for biochemical analysis. Multiple copies of target genes with apparently enhanced enzymatic yield can be achieved in *P. pastoris* (Teng *et al.*, 2015). This might be responsible for most of the excluded mutants in the final selection process. Therefore, making directed evolution in *S. cerevisiae* by using episomal vectors, and thereafter transferring the best variants to *P. pastoris* for overproduction in bioreactor might be a good option for future campaigns (Molina-Espeja *et al.*, 2015).

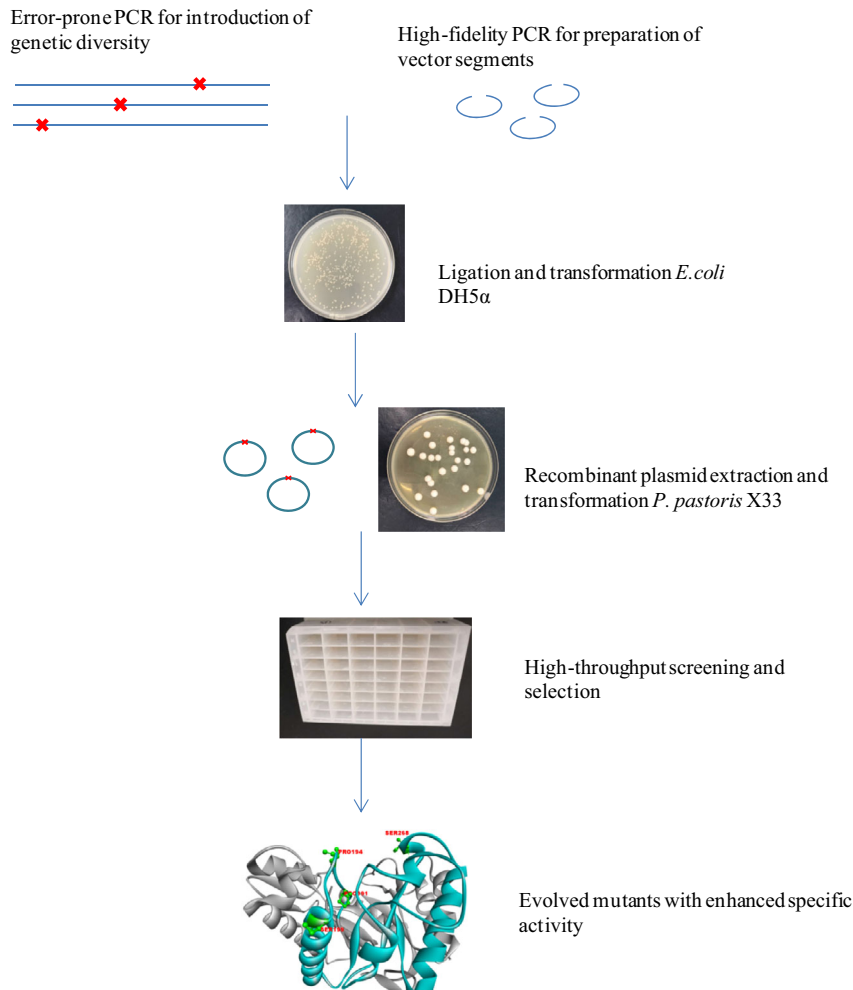


**Fig. 1.** Flowchart of directed evolution methodology used in this work.

*Biochemical characterization and kinetics of positive mutants*

Resolution of mutants by sodium dodecyl sulphate-polyacrylamide gel electrophoresis (SDS-PAGE) indicated that four positive mutants shared the same molecular weight (~55 kDa) with the wild-type enzyme (Fig. S2), and the molecular weight of deglycosylated mutants was about 45 kDa, which was 10 kDa lower than their glycosylation forms. This suggested that the glycosylation pattern of ManAK was not apparently altered by these four single-point mutations (P191 M, P194E, S199G and S286Q) (Cheng *et al.*, 2015; Liu *et al.*, 2021). As shown in Table 1, the specific activities of four mutants were improved, with 25.5%–60.9% enhancement compared with ManAKH. According to the temperature profiles (Fig. 2A and B), three mutants (P194E, S199G and S268Q) shared the same optimal temperature (75°C), while that of the P191 M mutant decreased to 70°C. It was also noteworthy that the relative activities of the four positive mutants at a low temperature range (40–65°C) were also apparently increased compared with ManAKH. This might be responsible for their enhanced specific activities at 37°C. As for their thermostability, the half-life ( $t_{1/2}$ ) parameters for enzymatic activity at 75°C of P191 M and P194E were decreased to 1.5 min and 15.6 min, respectively. By comparison, no significant changes to the thermostability of the S199G and S268Q mutants were detected. Compared with ManAKH, the pH properties of the four mutants were virtually unchanged (Fig. 2C and D). The optimal pH scales for enzymatic activity were 2–6, and these four mutants retained 80% of their initial activity after a 2-h pre-incubation at different buffered pHs (pH 2–8).

The kinetic parameters of the four mutants were calculated by non-linear regression analysis of experimentally obtained data (Fig. S3). As described in Table 2, P191 M, P194E and S268Q displayed significant enhancement of catalytic efficiencies, among which the  $k_{cat}/K_m$  values of P191 M increased to 438.8 ml s $^{-1}$ mg $^{-1}$  and 87.8% higher than that of ManAKH. The  $k_{cat}/K_m$  of

P194E decreased to 120.4 ml/s mg $^{-1}$ , mainly due to an increased  $K_m$  value (2.1 mg ml $^{-1}$ ).

*Structural–functional relationships of the four positive mutants*

In terms of spatial distribution, three mutation sites (P191, P194 and S268) were located in the catalytic core of ManAK (Fig. S4). Due to proline can adopt only a few configurations and restricts the configurations allowed for the preceding amino acid residue, mutation Pro→Xaa should increase the local flexibility of catalytic core, while in contrast, Glycine is the most flexible (Sriprapundh *et al.*, 2000; Vieille, 2001; Bu *et al.*, 2018). Meanwhile, enzyme-substrate docking analysis indicated that S268 could form a carbon hydrogen bond with mannotetrose (Liu *et al.*, 2020). Thus, their mutations probably perturb the catalytic characteristics of the enzyme. The mutation site, S199, was located outside the enzyme catalytic core; hence, it is likely that this site probably does not interact directly with the substrate. However, substituting S199 by the most flexible amino acid residue G could facilitate the flexibility of 187–198 loop. Improving the flexibility of the catalytic core is a widely adopted strategy for enhancing the catalytic activity of the enzyme (Huang *et al.*, 2014; Dong *et al.*, 2016; Zheng *et al.*, 2018). P191 M, P194E and S199G could directly or indirectly increase the flexibility of the catalytic core of enzyme, thus presumably facilitating the reaction at the catalytic residue E190. Similar result has been reported in the cellulase *GtCel5* from *Gloeophyllum trabeum* CBS 900.73, in which mutation N233G could increase the flexibility of loop 6 and enhance the interactions between enzyme and substrate (Zheng *et al.*, 2018). Besides, mutants showing a higher catalytic activity at low temperatures tend to have an improved flexibility of the structural catalytic components compared with their wild-type enzymes (Chiuri *et al.*, 2009). This might be an explanation for the improved specific activity of mutants at low temperatures. Similar results were also observed in two mutants (N233G and N233A) of the cellulase *GtCel5* (Zheng *et al.*, 2018).

The thermostability of the enzyme can be enhanced by decreasing the entropy of unfolding; thus, the mutations Gly→Xaa or Xaa→Pro have been frequently used in engineering thermostable enzymes (Vieille, 2001; Xie *et al.*, 2014; Yu *et al.*, 2017; Sun *et al.*, 2019). This might be responsible for the decreased thermostability of the three mutants (P191 M, P194E and S199G) in this work. Additionally, non-covalent bond changes could help to understand the thermostability shifting caused by the mutations (Fig. S5). Modelling analysis indicated that introducing a Met at the original site of P191 could probably substitute the weak carbon–hydrogen bond with a new sulphur- $\pi$  non-covalent bond, and additionally

**Table 1.** Comparison of properties of wild-type and designed ManAK mutants.

Name	$T_{opt}$ (°C)	$t_{1/2}$ (75°C) <sup>a</sup> (min)	pH <sub>opt</sub>	Specific activity (U mg $^{-1}$ )
ManAKH	75	40.9	2.0	200 ± 10
P191 M	70	1.5	2.0	290 ± 10
P194E	75	15.6	3.0	330 ± 11
S199G	75	38.7	3.0	318 ± 6
S268Q	75	47.9	2.0	255 ± 6

a.  $t_{1/2}$  was defined as the time needed for loss of half of the initial enzymatic activity at 75°C.

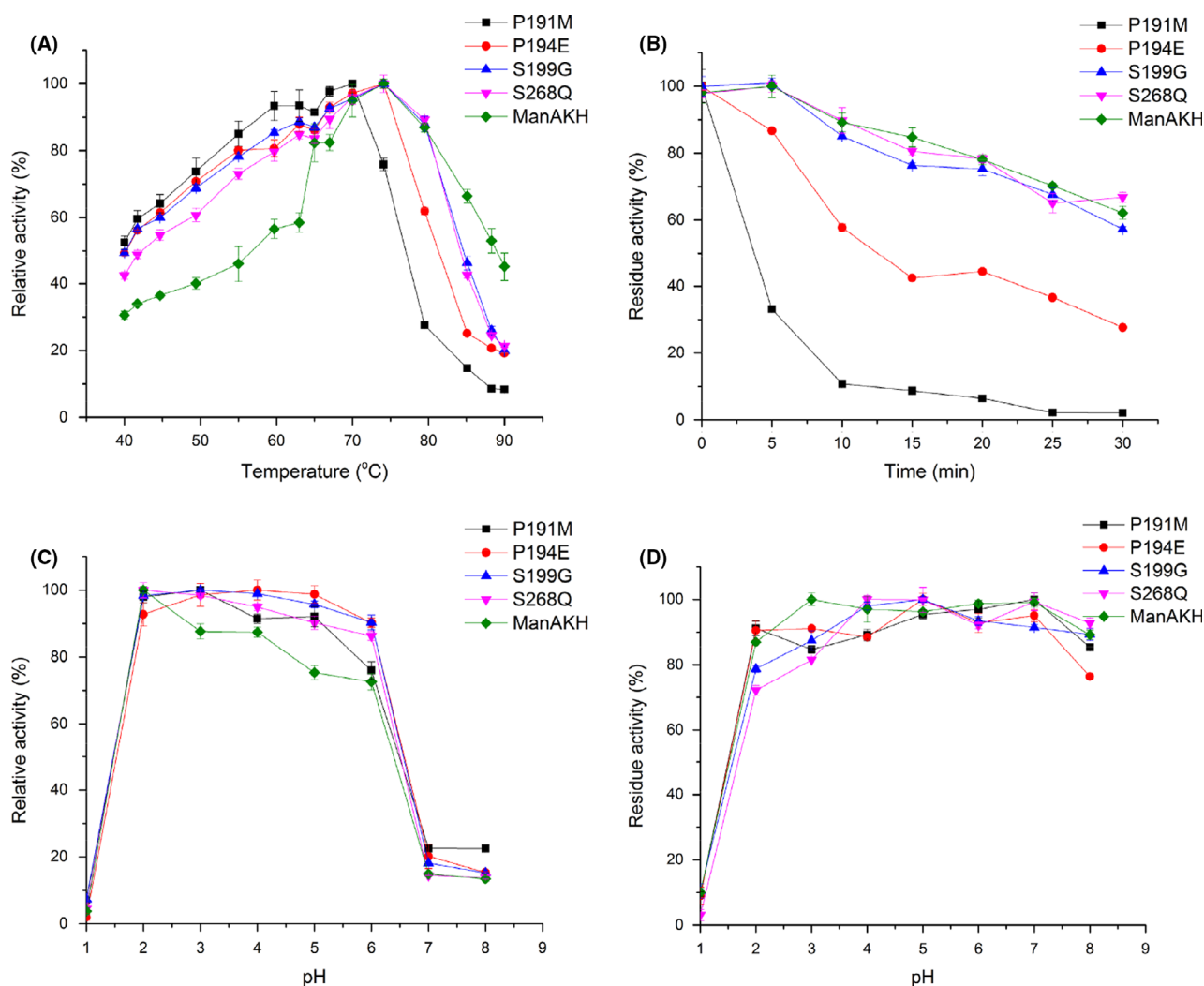


**Fig. 2.** Determinations of  $T_{opt}$  (A),  $t_{1/2}$  (75°C) (B),  $pH_{opt}$  (C) and pH stability (D) of positive mutants. pH stability was defined as the residue activity after a 2-h pre-incubation in different buffers (pH 1–8) at room temperature.

**Table 2.** Kinetic parameters of wild-type and designed ManAK mutants.

Name	$K_m$ (mg ml <sup>-1</sup> )	$V_{max}$ (U mg <sup>-1</sup> )	$k_{cat}$ (1 s <sup>-1</sup> )	$k_{cat}/K_m$ (ml s mg <sup>-1</sup> )
ManAKH	0.7 ± 0.1	255 ± 3	172.9	233.7
P191 M	0.6 ± 0.1	386 ± 8	254.5	438.8
P194E	0.9 ± 0.1	460 ± 7	303.1	356.6
S199G	2.1 ± 0.2	390 ± 13	255.2	120.4
S268Q	1.0 ± 0.1	380 ± 10	248.0	255.7

introduce two alkyl hydrophobic non-covalent bond interactions. However, this alteration could hardly compensate for the negative effect of entropy of unfolding on thermostability caused by a Pro → Xaa mutation. The P194E mutation could change a positive alkyl hydrophobic non-covalent bond interaction to a negative charge-charge interaction. The S199G mutation decreased a conventional hydrogen bond formed with D197, due to

S199 and D197 located at the same  $\alpha$ -helix secondary structure, which theoretically has a weak influence on the stability of the local tertiary structure. Mutation at site S199 is located at a different secondary structure from the catalytic residue E190; so the mutation effect on thermostability of S199G was apparently weaker than either P191 M or P194E. The S268G mutation could not bring either non-covalent bond interaction change or increased entropy of unfolding; therefore, no significant thermostability change was detected. There are a number of factors that could be responsible for the influences of point mutations on the thermostability of enzymes, such as types of amino acid and locations, glycosylation and disulfide bonds, non-covalent bond interactions (hydrogen bond, salt-bridge, hydrophobic interaction, and charge-charge interaction), and energy effects (Ding *et al.*, 2002; Xue *et al.*, 2012; Craig and Dombkowski, 2013; Yu *et al.*, 2017; Rigoldi *et al.*, 2018). Therefore,

the underlying mechanisms of point mutations on thermostability might be varying for each mutant and should be explained specifically.

#### Constructing a high-level expression strain using mutant *S199G*

A multi-copy strategy has been verified to be an efficient method for gaining high protein yield in *P. pastoris* (Ahmad *et al.*, 2014; Teng *et al.*, 2015). Furthermore, it is normally the initial strategy considered for constructing high-level expression strains (Zhou *et al.*, 2020). After three rounds of screenings, the recombinant strain (named X33VIIManAK<sup>S199G</sup>) showed the highest enzyme yield (~ 150 U ml<sup>-1</sup>) from a shake flask and was used for the following study.

#### Verification of the functions of AACC system in *P. pastoris*

The uracil auxotrophic strain (named X33VIIManAK<sup>S199G</sup>  $\Delta$ *ura3*) was constructed by using the 5-FOA method

(Nett and Gerngross, 2003) and used for the following genetic manipulation process (Fig.3). Phenotype identification and DNA sequencing analysis indicated that the *ura3* gene of X33VIIManAK<sup>S199G</sup> was successfully knocked out (Fig. S6). To test the gene deletion efficiency of the AACC system in X33VIIManAK<sup>S199G</sup>  $\Delta$ *ura3*, the target gene (*rox1*) encoding a heme-dependent transcription regulator was knocked out. As described in Fig. 4A, the target transformants generated from a second single crossover process displayed a stable uracil auxotrophic phenotype that could be conveniently screened by MDUF plates. The resulting mutant X33VIIManAK<sup>S199G</sup>  $\Delta$ *ura3* $\Delta$ *rox1* was achieved with 100% counter-selectable efficiency and 35.7% mutation efficiency, indicating that the AACC cassette could be successfully eliminated and the desired mutants could easily be selected.

To test the gene insertion/substitution efficiency, the gene *vgb* was designed to specifically integrate into the *rox1* locus of X33VIIManAK<sup>S199G</sup>  $\Delta$ *ura3*. As shown in Fig. 4C, all tested mutants from the second single

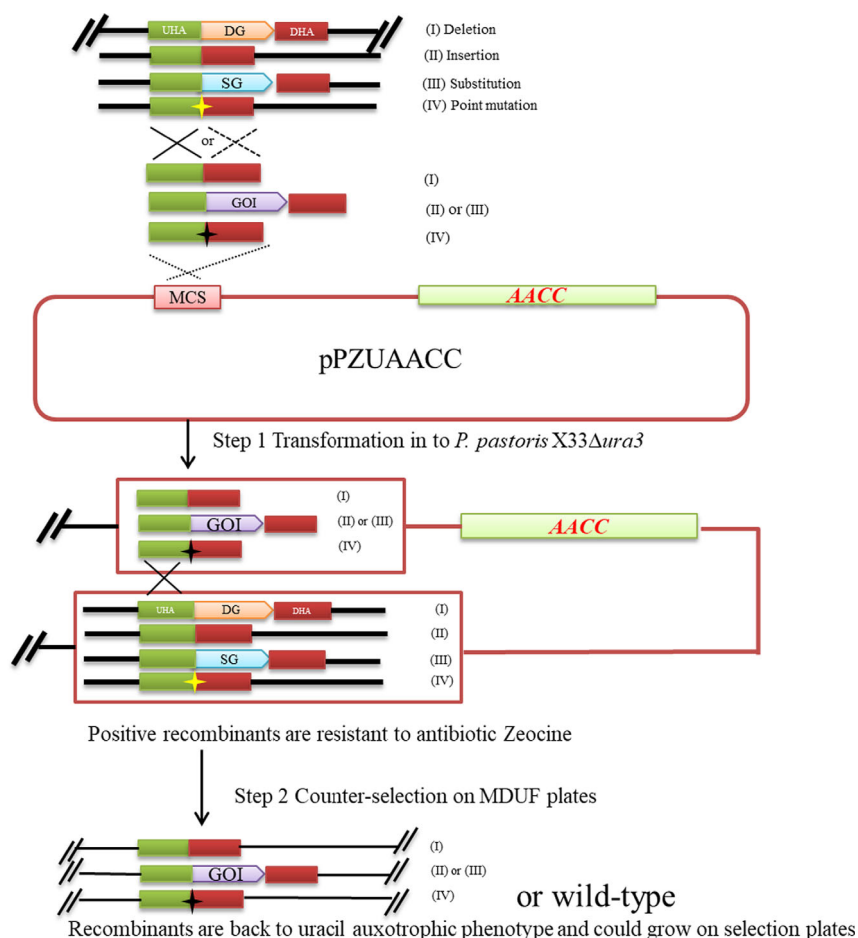


**Fig. 3.** Schematic illustration of AACC system for gene deletion, substitution, insertion and point mutation in *P. pastoris*. DG, SG and GOI represents deleted gene, substituted gene and gene of interest, respectively. Asterisk represents point mutation site.



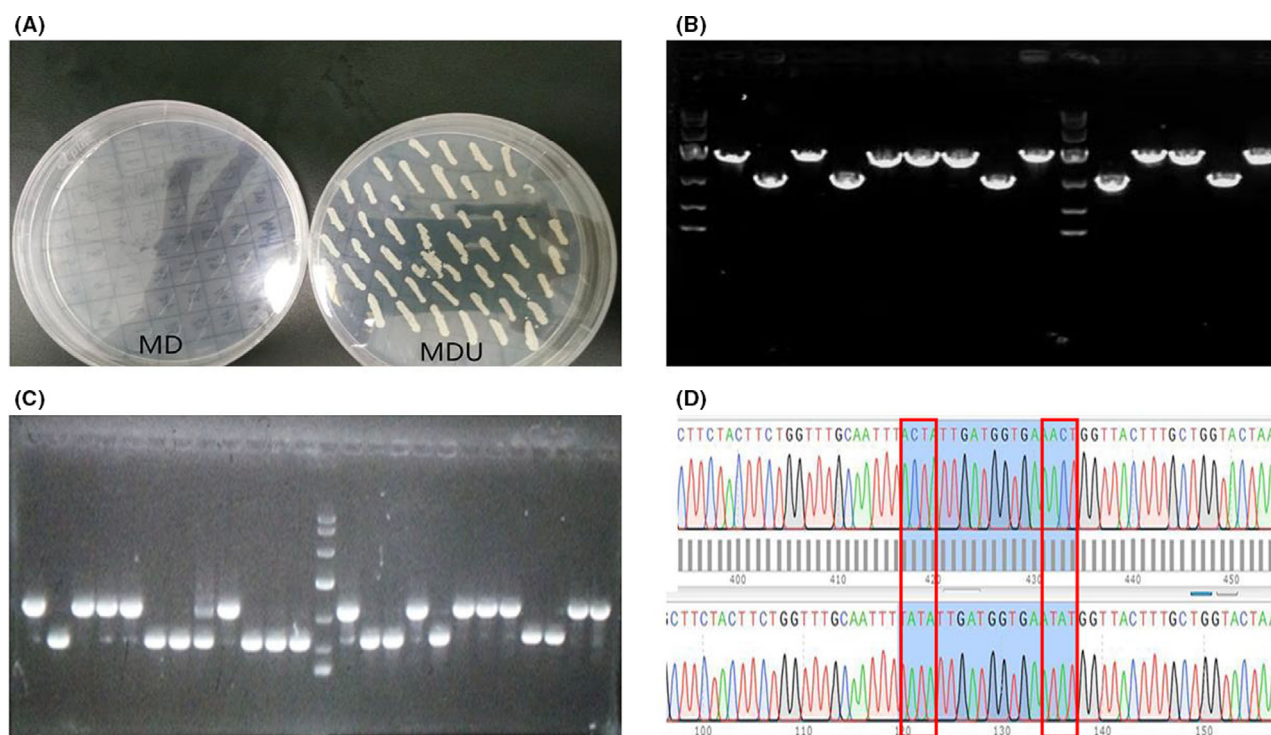


**Fig. 4.** Functional verification of AACC for gene deletion, insertion/substitution and point mutation.

A. Verification of the positive strain X33VIIManAK<sup>S199G</sup>Δura3Δrox1 by MD and MDU plates; (B) Verification of the positive strain X33VIIManAK<sup>S199G</sup>Δura3Δrox1 by PCR amplification; (C) PCR detection for *vgb* substitution at *rox1* locus of in X33VIIManAK<sup>S199G</sup>Δura3; (D) DNA sequencing for verification of introduced double mutation sites in ManAK. The theoretical molecular weight of PCR products for X33VIIManAK<sup>S199G</sup>Δura3Δrox1 decreased to 1000 bp from 2000 bp. Substituting gene *rox1* with *vgb* lead to the molecular weight of PCR product decreasing from about 1000bp to 500 bp. The molecular weight distributions (from bottom to top) of the DNA marker are 250, 500, 1000, 2000, 4000, 7000 and 10 000 bp, respectively.

crossover process were successful in eliminating the AACC cassette. Half (12/24) of the desired mutants (X33VIIManAK<sup>S199G</sup> Δura3Δrox1::*vgb*) were obtained, which was identical with the theoretical success rate (50%) for AACC system insertion/substitution of target genes.

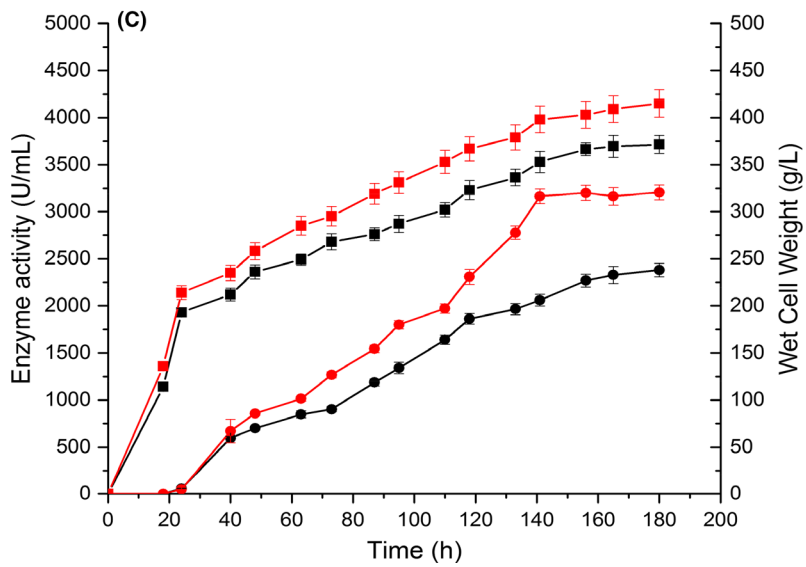
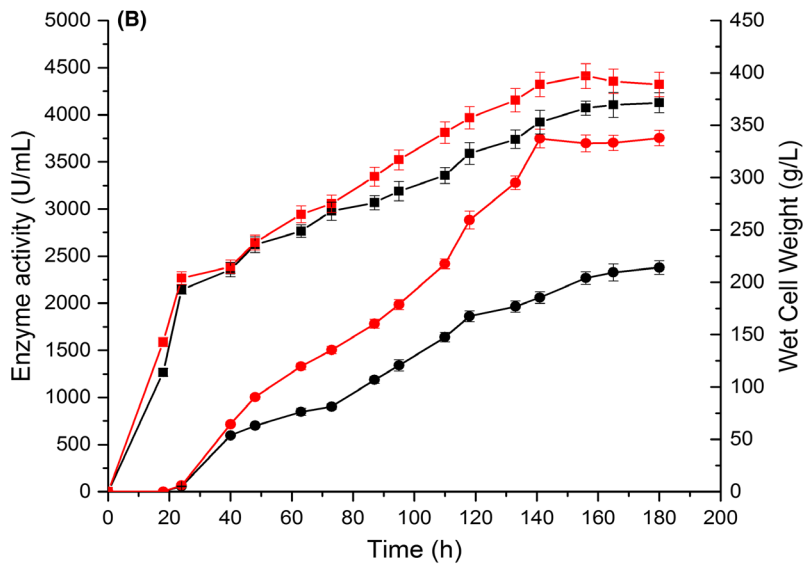
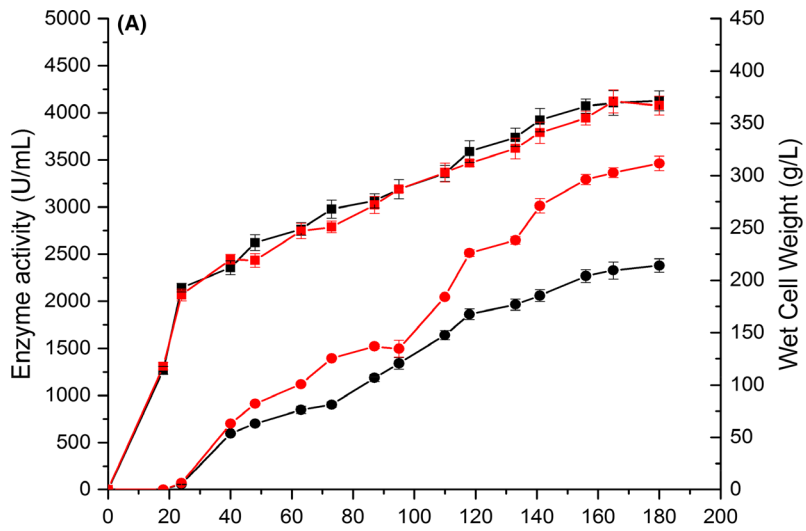
The mutation efficiency of the AACC system for introducing point mutations in the genome of *P. pastoris* was also examined. A single copy ManAK producing strain (X33IManAKΔura3) was adopted to introduce two single point mutations (T33Y and T38Y) simultaneously (Fig. 4 D). DNA-sequencing analysis gave a 58.3% (14/24) success rate for this process, which demonstrated the applicability of the AACC system in generating point mutations in *P. pastoris*. Overall, the AACC system developed in this work was proved to be multi-functional and an easy accessible tool for genetic manipulation of *P. pastoris*.

#### Effects of *rox1* deletion and/or Vhb coexpression on enzyme yields

It has been verified that intracellular heme levels and the transcription regulator Rox1p are two crucial factors

correlated with recombinant protein yield in yeasts (Wang *et al.*, 2012; Stark *et al.*, 2015; Martínez *et al.*, 2016; Zhou *et al.*, 2020). Normally, the industrial HCDF process of *P. pastoris* (Mut<sup>+</sup>) is divided into two stages based on the DO levels. At the early stage of methanol induction (0–60 h), the DO level can be kept at 20% or higher, due to the relatively low cell weight and protein production strength. After that, DO often becomes a limitation for cell respiration and protein synthesis. Therefore, in this section, the gene *rox1* was knocked out to facilitate protein production during the aerobic stage, and haemoglobin Vhb was co-expressed to benefit oxygen delivery and respiration metabolism at the anaerobic stage.

The enzyme yield of recombinant strain X33VIIManAK<sup>S199G</sup> was apparently enhanced by the HCDF process. The maximum enzymatic activity reached 2380 U ml<sup>-1</sup> and the yield of crude protein was 8.42 g l<sup>-1</sup> after 180 h of fermentation. This enzymatic activity yield was 14.9 times higher than that from shake flasks. For evaluating the influences of a *rox1* deletion on enzyme production, a strain named X33VIIManAK<sup>S199G</sup> Δ*rox1* was constructed and subjected to the HCDF process. As indicated in Fig. 5, the *rox1* deletion strain displayed a





higher enzymatic activity than X33VIIManAK<sup>S199G</sup> throughout the entire methanol induction phase. The maximum enzymatic activity for X33ManAK<sup>S199G</sup>Δ*rox1* reached 3462 U ml<sup>-1</sup>, which was 1.5 times as high as that of X33VIIManAK<sup>S199G</sup>. In addition, the total extracellular protein yield of X33ManAK<sup>S199G</sup>Δ*rox1* was enhanced to 11.5 g l<sup>-1</sup>. However, no significant change of biomass yield was detected, which suggested that the *rox1* deletion only has a weak influence on cell growth (Liu *et al.*, 2015).

Co-expression of VHb in X33VIIManAK<sup>S199G</sup> could also enhance enzymatic activity in the HCDF process. The modified strain X33VIIManAK<sup>S199G</sup>*ura3*:VHb almost reached the highest enzymatic activity (3206 U ml<sup>-1</sup>) after 140 h, which was 24 h earlier than X33ManAK<sup>S199G</sup>. Furthermore, the final wet cell weight of X33VIIManAK<sup>S199G</sup>*ura3*:VHb reached 415 g l<sup>-1</sup>, which was higher than that of X33VIIManAK<sup>S199G</sup> at 363 g l<sup>-1</sup>. Compared with X33VIIManAK<sup>S199G</sup>, the X33VIIManAK<sup>S199G</sup>*ura3*:VHb tolerated a higher methanol feeding rate (8 vs. 5 ml l<sup>-1</sup> h<sup>-1</sup>) during the HCDF process. VHb can enhance oxygen uptake and promote ATP synthesis and respiratory efficiency, thus strengthen cell growth and protein synthesis (Stark *et al.*, 2015). When considering energy consumption as the major element in manufacturing costs, the shortened fermentation time of the HCDF process further improves the market competitiveness of industrial enzymes (Jahic *et al.*, 2006).

A combined strategy was also adopted to construct the improved enzyme production strain, X33VIIManAK<sup>S199G</sup>Δ*rox1*::VHb. As shown in Fig. 5C, the maximum enzymatic activity and total yield of X33VIIManAK<sup>S199G</sup>Δ*rox1*::VHb were further increased to 3753 U ml<sup>-1</sup> and 12.8 g l<sup>-1</sup>, respectively. The maximum enzymatic activity yield of X33VIIManAK<sup>S199G</sup>Δ*rox1*::VHb was nearly twice as much as that of ManAK in *P. pastoris* (Liu *et al.*, 2020). Moreover, X33VIIManAK<sup>S199G</sup>Δ*rox1*::VHb reached the high enzymatic activity at an earlier fermentation time than X33VIIManAK<sup>S199G</sup> and X33VIIManAK<sup>S199G</sup>Δ*rox1*, and displayed a positive effect on cell growth. This indicated that deletion of *rox1* combining with co-expression of VHb was a feasible way to gain high protein yield in *P. pastoris*. Co-expression of VHb in X33VIIManAK<sup>S199G</sup>Δ*rox1* could further enhance the enzyme yield by 8.4%, however, when X33VIIManAK<sup>S199G</sup> was co-expressed with VHB, the enzyme activity was increased by 34.7%

compared with X33VIIManAK<sup>S199G</sup>. This mainly because the production of secreted protein in *P. pastoris* was restricted by several factors, such as limits in transcription and translation, incomplete protein folding and inefficient extracellular secretion capacities (Ahmad *et al.*, 2014). The enzyme production will reach its limit at a specific condition, where further optimizing the oxygen uptake of the strain will not enhance the enzyme yield any further (Li *et al.*, 2015).

In summary, a directed evolution methodology was adopted to improve the specific activity of ManAK at 37°C whilst retaining good thermostability and acidic resistance. Equally important, an easily accessible, multi-functional and scarless genetic manipulation system (AACC) was implemented to enhance enzymatic production in *P. pastoris* by knocking out gene *rox1* and co-expressing VHb. The maximum enzymatic activity of X33VIIManAK<sup>S199G</sup>Δ*rox1*::VHb was increased to 3753 U ml<sup>-1</sup>, which was nearly twice as much as the maximum production of ManAK in *P. pastoris*. Consequently, this study provides a systematic and effective method for improving the enzymatic activity yield of industrial enzymes in *P. pastoris* and promotes the application of ManAK in feed additives.

## Experimental procedures

### Materials

The main strains and plasmids ordered or constructed in this study are listed in Table S1. The main media used in this study were listed in Table S2. The gene encoding ManAK has been deposited in GenBank, with accession number MN539024. The Instant error-prone PCR Kit (TIANDZ, Beijing, China) was used for construction of a mutation library. All other chemicals and reagents ordered in this work were of analytical grade.

### Mutation library construction and high throughput screening

The mutation library of ManAK was constructed according to the instructions of the Instant error-prone PCR Kit, and the mutation rate was controlled at 2.0 base substitutions per gene. The expression plasmid pPICZαA was linearized by Superfidelity Phata Max polymerase (Vazyme, Jiangsu, China) and purified using a Cycle-pure kit (Omega, GA, USA) for ligation with purified

**Fig. 5.** Evaluation of *rox1* deletion and VHb co-expression on enzymatic activity yield of ManAK<sup>S199G</sup> in the HCDF process. A. Comparison of enzymatic activity and wet cell weight for X33VIIManAK<sup>S199G</sup>Δ*rox1* and X33VIIManAK<sup>S199G</sup>; (B) Comparison of enzymatic activity and wet cell weight for X33VIIManAK<sup>S199G</sup>*ura3*:VHb and X33VIIManAK<sup>S199G</sup>; (C) Comparison of enzymatic activity and wet cell weight for X33VIIManAK<sup>S199G</sup>Δ*rox1*::VHb and X33VIIManAK<sup>S199G</sup>. The enzymatic activity and wet cell weight were marked as circles (○) and squares (□), respectively. The fermentation data for the X33VIIManAK<sup>S199G</sup> was marked in black, and that for the other strains was marked in red.

error-prone PCR products by ClonExpress® II One Step Cloning Kit (Vazyme). Then, the recombinant plasmids were transformed into DH5 $\alpha$  competent cells for propagation. After that, all the clones selected on LB plates (Zeocin, 25  $\mu\text{g ml}^{-1}$ ) were washed out for the plasmids and extracted using an *E. coli* plasmid extraction kit (Omega). Finally, extracted plasmids were linearized by *SacI* restriction enzyme (Thermo Scientific, Waltham, MA, USA) and transformed into *P. pastoris* X33 for high throughput screening of high specific activity mutants.

High throughput screening was performed in 48-well deep plates containing 0.8-ml liquid BMGY medium per cell. The mutation library underwent three rounds of screening in accordance with a previously reported method (Zhang *et al.*, 2019). The positive variants selected in the first round of screening were further confirmed by two consecutive re-screenings in 48-well deep plates and 100-ml shake flasks, respectively. The transformants with apparently enhanced enzymatic activity (> 20%) when compared with the single-copy strain X331ManAK, were selected for enzyme preparation, purification and identification analysis.

#### Enzyme activity assay and biochemical identification of mutants

Enzymatic activity was assayed at 37°C, pH 5.5 according to 3,5- dinitrosalicylic acid (DNS) method (Miller, 1959). The reaction system containing 40- $\mu\text{l}$  diluted enzyme and 40- $\mu\text{l}$  0.6% (w/v) locust bean gum was firstly incubated at 37°C for 30 min, then, 100  $\mu\text{l}$  DNS reagent was added to terminate the reaction. After boiling at 100°C for 10min, 150- $\mu\text{l}$  reaction mixture was transferred to 96-well-ELISA plates for absorbance measurement at 540 nm using a microplate reader MultiskanFC (Thermo Scientific). One unit (U) of  $\beta$ -mannanase activity was defined as the amount of enzyme needed to produce 1  $\mu\text{mol}$  of reducing sugars per min.

All the enzymes were purified by a Ni-affinity chromatographic method using a Ni sepharose 6 FF column (GE Healthcare, USA) according to the manufacturer's instructions. A more detailed procedure for this has been well developed and described previously (Liu *et al.*, 2013). The protein concentration was determined according to the Bradford method (Bradford, 1976).

For overall evaluation of the effects of mutation upon the enzyme, basic biochemical properties, including optimum temperature ( $T_{\text{opt}}$ ), half-life ( $t_{1/2}$ ) of inactivation at 75°C, optimal pH ( $\text{pH}_{\text{opt}}$ ), pH stability and kinetic parameters, were performed in compliance with our previously published work (Liu *et al.*, 2021). Specifically,  $T_{\text{opt}}$  was determined by measuring the relative activities of enzymes at various temperatures ranging from 40°C–90°C at intervals of 5°C. The  $t_{1/2}$  value was

measured by detecting the residue activity of the enzyme pre-incubated at 75°C for different time intervals (5, 10, 15, 20, 25, and 30 min) and calculated by Eq. (1) (Yu *et al.*, 2017).

$$t_{1/2} = \ln(2)/k_d \quad (1)$$

where the first-order deactivation rate constant ( $k_d$ ) was determined by linear regression of  $\ln$  (residues activity) versus the pre-incubation time ( $t$ ) at 75°C. Kinetic parameters of enzymes were determined by measuring enzyme activity at different substrate concentrations (0.1–10  $\text{mg ml}^{-1}$  locust bean gum).  $K_m$  and  $V_{\text{max}}$  were calculated plotting initial velocity versus substrate concentration (Michaelis-Menten plot) (Ramesh *et al.*, 2019).

#### Modelling analysis of mutants

The three-dimensional structures of mutants were automatically modelled using the Phyre<sup>2</sup> program with reference to a reported crystal structure of ManBK (PDB code: 3WH9; 95% identity) (Kelley *et al.*, 2015). Non-covalent bond interaction analysis was performed by Discovery studio 2018 software. PyMOL software (version 1.7.2; Delano Scientific, San Carlos, CA, USA) was used for figures production of publication quality.

#### High-level expression strain construction and HCDF process

The liquid post-transformational vector amplification (PTVA) method was used to construct multi-copy strains in *P. pastoris*. Briefly, the recombinant expression plasmid pPIC9k-ManAK<sup>S199G</sup> was linearized by *SacI* and electro-transformed into *P. pastoris* X33. Then, the transformants underwent continuous cultivation in YPD liquid medium containing a series of concentrations (0.5, 1.0, 2.0, and 3.0  $\text{mg ml}^{-1}$ ) of the antibiotic G418. Finally, the transformants were cultured in 3.0  $\text{mg ml}^{-1}$  antibiotic for 24 h, diluted, and then spread on the YPD solid plates containing the same concentration of G418. Approximate 1000 clones were further screened to gain high-level expression strains according to a previously reported method (Zhang *et al.*, 2019). The copy number of the selected high-level expression strain was determined by a quantitative PCR method according to a published method (Yu *et al.*, 2020).

The HCDF process was conducted in a 7-l fermentor according to *Pichia* fermentation protocols (Invitrogen). In detail, 200 ml of prepared seeds in shake flasks were transformed into the fermentor containing 3 l basal salt medium and 12 ml PTM1 trace salts solutions. The entire process was divided into three stages (Glycerol batch, Glycerol fed-batch, and methanol fed-batch) under constant fermentation temperature and pH conditions

( $29.5 \pm 0.5^\circ\text{C}$  and  $\text{pH } 4.9 \pm 0.1$ ). During the methanol fed-batch stage, the accumulation of methanol was detected by the dissolve oxygen (DO) spike method, and the feeding rate of methanol was adjusted to maintain a stable growth state for enzyme production. The DO could be kept higher than 20% in the former 60 h of methanol fed-batch process, after that, it becomes lower due to the limitations of instruments and high biomass. The entire HCDF process was sustained for about 180 h, and samples at different time points were collected and analysed.

#### Construction of the AACC plasmids and recombinant plasmids

Relevant properties and resources of necessary plasmids and genes are listed in Table S1. All of the primers used in recombinant plasmid construction were automatically designed by CE Design Version 1.04 software (Vazyme). The counter-selection system AACC was constructed by replacing the AOX1 expression cassette in pPICZ $\alpha$ A plasmid with an URA3 expression cassette, which was amplified from the genome of *P. pastoris*. The knock-out plasmid pPZUAACC $\Delta$ rox1 was constructed by incorporating the upper homolog arm (UHA) and down homolog arm (DHA) of gene *rox1* to the 5'-end of the URA3 expression cassette. The knock-in plasmid pPZUAACC $\Delta$ rox1::VHb was constructed by inserting a VHb expression cassette ( $P_{\text{AOX1}}::\text{vgb}$ ) between UHA and DHA of pPZUAACC $\Delta$ rox1 (Fig. S1). The substitution plasmid pPZUAACC $\Delta$ rox1::vgb was constructed by inserting the *vgb* gene between the UHA and DHA of pPZUAACC $\Delta$ rox1. Point mutation plasmids pPZUAACCManAK<sup>T33Y+ T38Y</sup> were obtained by incorporating ManAK<sup>T33Y+ T38Y</sup> to the 5'-end of the URA3 expression cassette. The plasmid pPICZUura3::VHb was constructed by inserting a VHb expression cassette ( $P_{\text{AOX1}}::\text{vgb}$ ) to the 5'-end of a URA3 expression cassette that could be used as a DHA for double crossover recombination. The 1000 bp DNA sequence upstream of the URA3 expression cassette in the genome of *P. pastoris* was selected as the UHA.

#### Transformation and screening genetic modified strains

X33VIIManAK<sup>S199G</sup> $\Delta$ ura3 and X33IManAK $\Delta$ ura3 were obtained by deleting *ura3* in the genome of X33IManAK and X33VIIManAK<sup>S199</sup>, respectively. In detail, a knock-out fragment of *ura3* was transformed into X33IManAK and X33VIIManAK<sup>S199</sup> and screened on MDUF plates. The surviving clones underwent further selection on MD and MDU plates. Clones able to only grow on MDU plates were selected for DNA sequencing to verify the sequence accuracy. X33VIIManAK<sup>S199G</sup> $\Delta$ ura3 $\Delta$ rox1,

X33ManAK<sup>S199G</sup> $\Delta$ ura3 $\Delta$ rox1::vgb, and X33IManAK<sup>T33Y+ T38Y</sup> $\Delta$ ura3 were constructed by transforming pPZUAACC $\Delta$ rox1, pPZUAACC $\Delta$ rox1::vgb, and pPZUAACCManAK<sup>T33Y+ T38Y</sup> into X33VIIManAK<sup>S199G</sup> $\Delta$ ura3 and X33IManAK $\Delta$ ura3, respectively. The transformants were firstly screened on YPDZ plates (Zeocin 100  $\mu\text{g ml}^{-1}$ ). PCR amplification of target DNA segments with specifically designed primers was then undertaken to ensure that the right recombinant was present within the genome of *P. pastoris*. Positive transformants were inoculated into YPD liquid medium and cultured at 30°C and 220 rpm overnight for inducing the elimination of the AACC cassette. Then, the culture was diluted  $10^5$ – $10^6$ , and spread on MDUF plates for the counter-selection process.

X33VIIManAK<sup>S199G</sup>  $\Delta$ rox1 and X33ManAK<sup>S199G</sup>  $\Delta$ rox1::VHb were constructed by transforming the URA3 expression cassette into X33VIIManAK<sup>S199G</sup> $\Delta$ ura3 $\Delta$ rox1 and X33ManAK<sup>S199G</sup> $\Delta$ ura3 $\Delta$ rox1::VHb, and clones selected on MD plates. Positive transformants were further identified by DNA sequencing of target segments. The segment between two homolog arms in plasmid pPICZUura3::VHb was amplified and transformed into X33IManAK $\Delta$ ura3 competent cells. Positive transformants (named X33VIIManAK<sup>S199G</sup>ura3::VHb) were selected on MD plates and further identified by DNA sequencing of the target segment.

#### Scheme for genome modifications using the AACC system

The universal vector (pPZUAACC) for genome modification in X33VIIManAK<sup>S199G</sup>  $\Delta$ ura3 was constructed by substituting the original AOX1 expression cassette in pPICZ $\alpha$ A, with an URA3 expression cassette. Designed DNA fragments for genetic manipulation can be inserted upstream of the URA3 expression cassette and transformed into *E. coil*, firstly for recombinant plasmid (pPZUAACCx) verification and propagation. The recombinant plasmid was then linearized at sites of homology arms, to improve the single crossover recombination efficiency, and then transformed into X33VIIManAK<sup>S199G</sup> by electro-transformation. The positive clones with a single crossover event were screened on YPD plates with Zeocin, and further identified by PCR amplification and DNA sequencing.

A counter-selection process was performed by inoculating positive clones into YPD liquid medium without antibiotic. Then, target transformants were achieved after eliminating the AACC system by second single crossover events screened on MDUF plates. Finally, the correctness of the AACC system excursion was identified by checking the uracil auxotrophic phenotype and antibiotic resistance on corresponding selection plates. The

resulting mutants were then identified by DNA sequencing of the mutated sites in the genome.

### Acknowledgements

We thank Dr. Zhuoya Wang at Centre for High Performance Computing and System Simulation, Pilot National Laboratory for Marine Science and Technology, Qingdao, China for assisting modelling analysis in this work.

### Funding Information

National Key Research and Development (R& D) Program of China (2019YFD0901805), and National Nature Science Fund of China (31872893).

### Conflict of interest

The authors declare that they have no conflict of interest.

### Ethical approval

This article does not contain any studies with human participants or animals performed by any of the authors.

### References

- Ahmad, M., Hirz, M., Pichler, H., and Schwab, H. (2014) Protein expression in *Pichia pastoris*: Recent achievements and perspectives for heterologous protein production. *Appl Microbiol Biotechnol* **98**: 5301–5317.
- Bradford, M.M. (1976) A rapid and sensitive method for the quantitation of microgram quantities of protein utilizing the principle of protein-dye binding. *Anal Biochem* **72**: 248–254.
- Bu, Y., Cui, Y., Peng, Y., Hu, M., Tian, Y., Tao, Y., and Wu, B. (2018) Engineering improved thermostability of the GH11 xylanase from *Neocallimastix patriciarum* via computational library design. *Appl Microbiol Biotechnol* **102**: 3675–3685.
- Cheng, Y.S., Chen, C.C., Huang, J.W., Ko, T.P., Huang, Z., and Guo, R.T. (2015) Improving the catalytic performance of a GH11 xylanase by rational protein engineering. *Appl Microbiol Biotechnol* **99**: 9503–9510.
- Chiuri, R., Maiorano, G., Rizzello, A., del Mercato, L.I., Cingolani, R., Rinaldi, R., *et al.* (2009) Exploring local flexibility/rigidity in psychrophilic and mesophilic carbonic anhydrases. *Biophys J* **96**: 1586–1596.
- Choi, J.M., Han, S.S., and Kim, H.S. (2015) Industrial applications of enzyme biocatalysis: Current status and future aspects. *Biotechnol Adv* **33**: 1443–1454.
- Craig, D.B., and Dombkowski, A.A. (2013) Disulfide by Design 2.0: a web-based tool for disulfide engineering in proteins. *BMC Bioinformatics* **14**.
- Dhawan, S., and Kaur, J. (2007) Microbial mannanases: an overview of production and applications. *Crit Rev Biotechnol* **27**: 197–216.
- Ding, F., Dokholyan, N.V., Buldyrev, S.V., Stanley, H.E., and Shakhnovich, E.I. (2002) Direct molecular dynamics observation of protein folding transition state ensemble. *Biophys J* **83**: 3525–3532.
- Dong, H., and Zhang, D. (2014) Current development in genetic engineering strategies of *Bacillus* species. *Microb Cell Fact* **13**: 1–11.
- Dong, Y.H., Li, J.F., Hu, D., Yin, X., Wang, C.J., Tang, S.H., and Wu, M.C. (2016) Replacing a piece of loop-structure in the substrate-binding groove of *Aspergillus usamii*  $\beta$ -mannanase, AuMan5A, to improve its enzymatic properties by rational design. *Appl Microbiol Biotechnol* **100**: 3989–3998.
- Fischer, J.E., and Glieder, A. (2019) Current advances in engineering tools for *Pichia pastoris*. *Curr Opin Biotechnol* **59**: 175–181.
- Gübitz, G.M., Lischnig, T., Stebbing, D., and Saddler, J.N. (1997) Enzymatic removal of hemicellulose from dissolving pulps. *Biotechnol Lett* **19**: 491–495.
- Huang, J.-W., Chen, C.-C., Huang, C.-H., Huang, T.-Y., Wu, T.-H., Cheng, Y.-S., *et al.* (2014) Improving the specific activity of  $\beta$ -mannanase from *Aspergillus niger* BK01 by structure-based rational design. *Biochim Biophys Acta - Proteins Proteomics* **1844**: 663–669.
- Jahic, M., Veide, A., Charoenrat, T., Teeri, T., and Enfors, S.O. (2006) Process technology for production and recovery of heterologous proteins with *Pichia pastoris*. *Biotechnol Prog* **22**: 1465–1473.
- Kan, S.B.J., Huang, X., Gumulya, Y., Chen, K., and Arnold, F.H. (2017) Genetically programmed chiral organoborane synthesis. *Nature* **552**: 132–136.
- Kan, S.B.J., Lewis, R.D., Chen, K., and Arnold, F.H. (2016) Directed evolution of cytochrome c for carbon-silicon bond formation: Bringing silicon to life. *Science (80-)* **354**: 1048–1051.
- Kelley, L.A., Mezulis, S., Yates, C.M., Wass, M.N., and Sternberg, M.J.E. (2015) The Phyre2 web portal for protein modeling, prediction and analysis. *Nat Protoc* **10**: 845–858.
- Li, C., Lin, Y., Zheng, X., Pang, N., Liao, X., Liu, X., *et al.* (2015) Combined strategies for improving expression of *Citrobacter amalonaticus* phytase in *Pichia pastoris*. *BMC Biotechnol* **1**–11.
- Li, X., Liu, Z., Wang, G., Pan, D., Jiao, L., and Yan, Y. (2016) Overexpression of *Candida rugosa* lipase Lip1 via combined strategies in *Pichia pastoris*. *Enzyme Microb Technol* **82**: 115–124.
- Lin, Z., Deng, B., Jiao, Z., Wu, B., Xu, X., Yu, D., and Li, W. (2013) A versatile mini-mazF-cassette for marker-free targeted genetic modification in *Bacillus subtilis*. *J Microbiol Methods* **95**: 207–214.
- Liu, L., Zhang, Y., Liu, Z., Petranovic, D., and Nielsen, J. (2015) Improving heterologous protein secretion at aerobic conditions by activating hypoxia-induced genes in *Saccharomyces cerevisiae*. *FEMS Yeast Res* **15**: 1–10.
- Liu, Z., Li, G., Mo, Z., and Mou, H. (2013) Molecular cloning, characterization, and heterologous expression of a new  $\kappa$ -carrageenase gene from marine bacterium *Zobellia* sp. ZM-2. *Appl Microbiol Biotechnol* **97**: 10057–10067.
- Liu, Z., Liang, Q., Wang, P., Kong, Q., Fu, X., and Mou, H. (2021) Improving the kinetic stability of a

- hyperthermostable  $\beta$ -mannanase by a rationally combined strategy. *Int J Biol Macromol* **167**: 405–414.
- Liu, Z., Ning, C., Yuan, M., Yang, S., Wei, X., Xiao, M., et al. (2020) High-level expression of a thermophilic and acidophilic  $\beta$ -mannanase from *Aspergillus kawachii* IFO 4308 with significant potential in mannoooligosaccharide preparation. *Bioresour Technol* **295**: 122257.
- Malgas, S., van Dyk, J.S., and Pletschke, B.I. (2015) A review of the enzymatic hydrolysis of mannans and synergistic interactions between  $\beta$ -mannanase,  $\beta$ -mannosidase and  $\alpha$ -galactosidase. *World J Microbiol Biotechnol* **31**: 1167–1175.
- Markel, U., Essani, K.D., Besirlioglu, V., Schiffels, J., Streit, W.R., and Schwaneberg, U. (2020) Advances in ultra-high-throughput screening for directed enzyme evolution. *Chem Soc Rev* **49**: 233–262.
- Martínez, J.L., Petranovic, D., and Nielsen, J. (2016) Heme metabolism in stress regulation and protein production: From Cinderella to a key player. *Bioengineered* **7**: 112–115.
- Miller, G.L. (1959) Use of dinitrosalicylic acid reagent for determination of reducing sugar. *Anal Chem* **31**: 426–428.
- Molina-Espeja, P., Ma, S., Mate, D.M., Ludwig, R., and Alcalde, M. (2015) Tandem-yeast expression system for engineering and producing unspecific peroxygenase. *Enzyme Microb Technol* **73–74**: 29–33.
- Nett, J.H., and Gemgross, T.U. (2003) Cloning and disruption of the PpURA5 gene and construction of a set of integration vectors for the stable genetic modification of *Pichia pastoris*. *Yeast* **20**: 1279–1290.
- Prielhofer, R., Maurer, M., Klein, J., Wenger, J., Kiziak, C., Gasser, B., and Mattanovich, D. (2013) Induction without methanol: Novel regulated promoters enable high-level expression in *Pichia pastoris*. *Microb Cell Fact* **12**: 1–10.
- Ramesh, V., Harmer, N.J., and Vivoli Vega, M. (2019) Reaction chemical kinetics in biology. *Biomol Bioanal Tech* 179–217.
- Rigoldi, F., Donini, S., Redaelli, A., Parisini, E., and Gautieri, A. (2018) Review: engineering of thermostable enzymes for industrial applications. *APL Bioeng* **2**: 11501.
- Sachslehner, A., Foidl, G., Foidl, N., Gubitzi, G., and Haltrich, D. (2000) Hydrolysis of isolated coffee mannan and coffee extract by mannanases of *Sclerotium rolfsii*. *J Biotechnol* **80**: 127–134.
- Schwarzshans, J.P., Wibberg, D., Winkler, A., Luttermann, T., Kalinowski, J., and Friehs, K. (2016) Integration event induced changes in recombinant protein productivity in *Pichia pastoris* discovered by whole genome sequencing and derived vector optimization. *Microb Cell Fact* **15**: 1–15.
- Sriprapundh, D., Vieille, C., and Zeikus, J.G. (2000) Molecular determinants of xylose isomerase thermal stability and activity: analysis of thermozymes by site-directed mutagenesis. *Protein Eng* **13**: 259–265.
- Srivastava, P.K., and Kapoor, M. (2017) Production, properties, and applications of endo- $\beta$ -mannanases. *Biotechnol Adv* **35**: 1–19.
- Srivastava, P.K., Panwar, D., Prashanth, K.V.H., and Kapoor, M. (2017) Structural characterization and in vitro fermentation of  $\beta$ -mannooligosaccharides produced from locust bean gum by GH-26 endo- $\beta$ -1,4-Mannanase (ManB-1601). *J Agric Food Chem* **65**: 2827–2838.
- Stark, B.C., Pagilla, K.R., and Dikshit, K.L. (2015) Recent applications of Vitreoscilla hemoglobin technology in bio-product synthesis and bioremediation. *Appl Microbiol Biotechnol* **99**: 1627–1636.
- Sun, Z., Liu, Q., Qu, G., Feng, Y., and Reetz, M.T. (2019) Utility of B-factors in protein science: interpreting rigidity, flexibility, and internal motion and engineering thermostability. *Chem Rev* **119**: 1626–1665.
- Tang, Z., Jin, W., Sun, R., Liao, Y., Zhen, T., Chen, H., et al. (2018) Improved thermostability and enzyme activity of a recombinant phyA mutant phytase from *Aspergillus niger* N25 by directed evolution and site-directed mutagenesis. *Enzyme Microb Technol* **108**: 74–81.
- Teng, D., Xi, D., Zhang, J., Wang, X., Mao, R., Zhang, Y., and Wang, J. (2015) Multiple copies of the target gene enhances plectasin secretion in *Pichia pastoris* X-33. *Process Biochem* **50**: 553–560.
- Tolner, B., Smith, L., Begent, R.H.J., and Chester, K.A. (2006) Production of recombinant protein in *Pichia pastoris* by fermentation. *Nat Protoc* **1**: 1006–1021.
- Vieille, C., and Zeikus, G.J. (2001) Hyperthermophilic enzymes: sources, uses, and molecular mechanisms for thermostability. *Microbiol Mol Biol Rev* **65**: 1–43.
- Vocadlo, D.J., and Davies, G.J. (2008) Mechanistic insights into glycosidase chemistry. *Curr Opin Chem Biol* **12**: 539–555.
- Vogl, T., Gebbie, L., Palfreyman, R.W., and Speight, R. (2018) Effect of plasmid design and type of integration event on recombinant protein expression in *Pichia pastoris*. *Appl Environ Microbiol* **84**.
- Wang, X., Sun, Y., Shen, X., Ke, F., Zhao, H., Liu, Y., et al. (2012) Intracellular expression of *Vitreoscilla* hemoglobin improves production of *Yarrowia lipolytica* lipase LIP2 in a recombinant *Pichia pastoris*. *Enzyme Microb Technol* **50**: 22–28.
- Wu, J., Deng, A., Sun, Q., Bai, H., Sun, Z., Shang, X., et al. (2018) Bacterial genome editing via a designed toxin–antitoxin cassette. *ACS Synth Biol* **7**: 822–831.
- Wu, J.M., and Fu, W.C. (2012) Intracellular co-expression of *Vitreoscilla* hemoglobin enhances cell performance and  $\beta$ -galactosidase production in *Pichia pastoris*. *J Biosci Bioeng* **113**: 332–337.
- Xie, Y., An, J., Yang, G., Wu, G., Zhang, Y., Cui, L., and Feng, Y. (2014) Enhanced enzyme kinetic stability by increasing rigidity within the active site. *J Biol Chem* **289**: 7994–8006.
- Xue, H., Zhou, J., You, C., Huang, Q., and Lu, H. (2012) Amino acid substitutions in the N-terminus, cord and  $\alpha$ -helix domains improved the thermostability of a family 11 xylanase XynR8. *J Ind Microbiol Biotechnol* **39**: 1279–1288.
- Yamabhai, M., Sak-Ubol, S., Srila, W., and Haltrich, D. (2016) Mannan biotechnology: from biofuels to health. *Crit Rev Biotechnol* **36**: 32–42.
- Yin, L.L., Yuan, H., Liu, C., He, B.o., Gao, S.-Q., Wen, G.-B., et al. (2018) A rationally designed myoglobin exhibits a catalytic dehalogenation efficiency more than 1000-fold that of a native dehaloperoxidase. *ACS Catal* **8**: 9619–9624.

- Yu, H., Yan, Y., Zhang, C., and Dalby, P.A. (2017) Two strategies to engineer flexible loops for improved enzyme thermostability. *Sci Rep* **7**: 1–15.
- Yu, Y., Liu, Z., Chen, M., Yang, M., Li, L., and Mou, H. (2020) Enhancing the expression of recombinant  $\kappa$ -carageenase in *Pichia pastoris* using dual promoters, co-expressing chaperones and transcription factors. *Biocatal Biotransform* **38**: 104–113.
- Zhang, G.Q., Dong, X.F., Wang, Z.H., Zhang, Q., Wang, H.X., and Tong, J.M. (2010) Purification, characterization, and cloning of a novel phytase with low pH optimum and strong proteolysis resistance from *Aspergillus ficuum* NTG-23. *Bioresour Technol* **101**: 4125–4131.
- Zhang, W., Liu, Z., Zhou, S., Mou, H., and Zhang, R. (2019) Cloning and expression of a  $\beta$ -mannanase gene from *Bacillus* sp. MK-2 and its directed evolution by random mutagenesis. *Enzyme Microb Technol* **124**: 70–78.
- Zhao, X., Zhou, J., Du, G., and Chen, J. (2020) Recent advances in the microbial synthesis of hemoglobin. *Trends Biotechnol* **39**: 286–297.
- Zheng, F., Tu, T., Wang, X., Wang, Y., Ma, R., Su, X., *et al.* (2018) Biotechnology for Biofuels Enhancing the catalytic activity of a novel GH5 cellulase Gt Cel5 from *Gloeophyllum trabeum* CBS 900 . 73 by site – directed mutagenesis on loop 6. *Biotechnol Biofuels* **11**: 1–13.
- Zhou, Q., Su, Z., Jiao, L., Wang, Y., Yang, K., Li, W., and Yan, Y. (2020) High-level production of a thermostable mutant of *yarrowia lipolytica* lipase 2 in *pichia pastoris*. *Int J Mol Sci* **21**: 279.

## Supporting information

Additional supporting information may be found online in the Supporting Information section at the end of the article.

**Fig. S1.** Schematic illustration for plasmids pZUACC, pZUAACC $\Delta$ rox1, and pZUAACC $\Delta$ rox1::VHb construction.

**Fig. S2.** SDS-PAGE analysis on specific activity enhanced mutants and their deglycosylated enzymes (A), and extracellular proteins during HCDF process (B). Line M: molecular weight standards for protein; Line 1-9: fermentation supernatant samples withdrawn at different time points (24, 29, 43, 63, 73, 87, 97, 111, and 120 h).

**Fig. S3.** Non-linear fitting plots of four mutants. a: P191M ( $R^2 = 0.99$ ); b: P194E ( $R^2 = 0.99$ ); c: S199G ( $R^2 = 0.92$ ); d: S268Q ( $R^2 = 0.98$ ).

**Fig. S4.** Overview on the distributions of four positive mutation sites on the tertiary structure of ManAK.

**Fig. S5.** Computational analysis on the non-covalent bonds alterations caused by single point mutation. A and a: P191M mutation effects on non-covalent bond interaction; B and b: P194E mutation effects on non-covalent bond interaction; C and c: P199G mutation effects on non-covalent bond interaction; D and d: S268Q mutation effects on non-covalent bond interaction. The blue dashed line, orange dashed line, yellow dashed line, black dashed line, and green dashed line indicates carbon hydrogen bond, alkyl hydrophobic non-covalent bond, sulfur- $\pi$  non-covalent bond, negative charge-charge interaction, and conventional hydrogen bond, respectively.

**Fig. S6.** Verification of *ura3* deletion in X33IManAK $\Delta$ ura3 and X33VIIManAK<sup>S199G</sup> $\Delta$ ura3 by PCR amplification. Gene *ura3* deletion led to the molecular weight of PCR product decreased from 2043 bp to 1247 bp. Line 1: X33IManAK; Line 2: X33VIIManAK; Line 3-6: X33IManAK $\Delta$ ura3; Line 7-10: X33VIIManAK<sup>S199G</sup> $\Delta$ ura3. The molecular weight distributions (from bottom to top) of DNA marker are 250, 500, 1000, 2000, 4000, 7000, and 10000 bp, respectively.

**Table S1.** Main strains, plasmids and genes used in this study.

**Table S2.** Main media used in this study.